

1

2 **Levetiracetam Modulates Brain Metabolic Networks and Transcriptomic Signatures in the 5XFAD**
3 **Mouse Model of Alzheimer's disease.**

4

5 Charles P. Burton¹, Evgeny J. Chumin^{1,2}, Alyssa Y. Collins¹, Scott A. Persohn¹, Kristen D. Onos³,
6 Ravi S. Pandey⁴, Sara K. Quinney⁵, and Paul R. Territo^{1,5}

7

8 **Affiliations:**

9 ¹ Stark Neurosciences Research Institute, Indiana University School of Medicine, Indianapolis IN 46202
10 USA

11 ² Department of Radiology and Imaging Sciences, Indiana University School of Medicine, Indianapolis IN
12 46202

13 ³ The Jackson Laboratory, Bar Harbor, ME 04609

14 ⁴ The Jackson Laboratory for Genomic Medicine, Farmington, CT 06032

15 ⁵ Department of Medicine, Division of Clinical Pharmacology, Indiana University School of Medicine,
16 Indianapolis IN 46202 USA

17

18 **CORRESPONDING AUTHOR:**

19 Paul R. Territo, Ph.D.

20 1345 West 16th Street, BRTC 308

21 Indianapolis, Indiana 46202

22 pterrito@iu.edu

23

24 **SHORT TITLE:** Levetiracetam Modulates Connectomics and Transcriptomics in 5XFAD Mice

25 **KEYWORDS:** Levetiracetam; Alzheimer's disease; 5XFAD; Connectomics

26

27 **ABSTRACT:**

28 *INTRODUCTION:* Subcritical epileptiform activity is associated with impaired cognitive function and is
29 commonly seen in patients with Alzheimer's disease (AD). The anti-convulsant, levetiracetam (LEV), is
30 currently being evaluated in clinical trials for its ability to reduce epileptiform activity and improve cognitive
31 function in AD. The purpose of the current study was to apply pharmacokinetics (PK), network analysis
32 of medical imaging, gene transcriptomics, and PK/PD modeling to a cohort of amyloidogenic mice to
33 establish how LEV restores or drives alterations in the brain networks of mice in a dose-dependent basis
34 using the rigorous preclinical pipeline of the MODEL-AD Preclinical Testing Core.

35 *METHODS:* Chronic LEV was administered to 5XFAD mice of both sexes for 3 months based on
36 allometrically scaled clinical dose levels from PK models. Data collection and analysis consisted of a
37 multi-modal approach utilizing ¹⁸F-FDG PET/MRI imaging and analysis, transcriptomic analyses, and
38 PK/PD modeling.

39 *RESULTS:* Pharmacokinetics of LEV showed a sex and dose dependence in C_{max} , CL/F, and $AUC_{0-\infty}$,
40 with simulations used to estimate dose regimens. Chronic dosing at 10, 30, and 56 mg/kg, showed ¹⁸F-
41 FDG specific regional differences in brain uptake, and in whole brain covariance measures such as
42 clustering coefficient, degree, network density, and connection strength (i.e. positive and negative). In
43 addition, transcriptomic analysis via nanoString showed dose-dependent changes in gene expression in
44 pathways consistent ¹⁸F-FDG uptake and network changes, and PK/PD modeling showed a
45 concentration dependence for key genes, but not for network covariance modeling.

46 *DISCUSSION:* This study represents the first report detailing the relationships of metabolic covariance
47 and transcriptomic network changes resulting from LEV administration in 5XFAD mice. Overall, our
48 results highlight non-linear kinetics based on dose and sex, where gene expression analysis
49 demonstrated LEV dose- and concentration- dependent changes, along with cerebral metabolism, and/or
50 cerebral homeostatic mechanisms relevant to human AD, which aligned closely with network covariance
51 analysis of ¹⁸F-FDG images. Collectively, this study show cases the value of a multimodal connectomic,
52 transcriptomic, and pharmacokinetic approach to further investigate dose dependent relationships in
53 preclinical studies, with translational value towards informing clinical study design.

54 INTRODUCTION

55 Subclinical epileptiform activity is commonplace in both mouse models of Alzheimer's Disease (AD) and
56 in the clinic [1, 2]. Recent work has shown that sustained expression of the calcium binding protein,
57 calbindin-D_{28K}, buffers cytosolic calcium in mouse models of AD, while healthy controls showed
58 decreased expression with age in subiculum dendrites, thus forming a molecular basis of epileptiform
59 activity in models of AD [3, 4]. Additional work has reported spike wave discharge activity in the 5XFAD
60 mouse model of AD, which is consistent with human AD epileptiform activity, where hippocampal
61 hyper-excitability has been observed in human *APOE*^{E4/E4} carriers [5]. Importantly, this activity has been
62 shown to localize to β-amyloid (Aβ) plaques, where neuronal dysregulation is thought to result from
63 impaired synaptic inhibition, thus driving aberrant excitatory activity. Neurons distal to the plaques show
64 abnormally low spike wave discharge activity [6], suggesting that Aβ plaque load may play an important
65 role in epileptiform formation. Provided this, anti-epileptic drugs have been considered as a possible
66 treatment paradigm and are hypothesized to attenuate synchronized hyperactivity in patients with AD [7].
67 One drug in particular, Levetiracetam (LEV), received FDA approval in 2000 for the treatment of seizures
68 and epilepsy in adults and adolescents [8]. Recent clinical trials administering LEV in AD patients have
69 found improved cognitive function in patients with epileptiform activity [9]. In humanized amyloid
70 precursor protein (*hAPP*) mice, LEV significantly reduced epileptiform activity in a dose-dependent
71 manner and halted disease progression [10]. Combined, these data suggest that LEV treatment may be
72 efficacious in attenuating disease progression in 5XFAD mice that overexpress Aβ and suggest that
73 prophylactic treatment with LEV may provide experimental evidence as a treatment for late onset AD
74 (LOAD) [6].

75 Clinically, hyper-excitability has been associated with seizures in AD patients [1, 11, 12]. This
76 phenomenon is also observed in AD mouse models such as 5XFAD and *APP/PS1* [13, 14]. LEV's acute
77 administration in amyloid mouse models has shown attenuation of abnormal spike wave activity [13],
78 while chronic treatment via continuous mini-pump infusion has been associated with the reversal of
79 synaptic loss and behavioral impairment in *hAPP* mice [10]. However, prior preclinical studies have not
80 fully characterized the pharmacokinetics (PK) of LEV and its impact on gene transcriptomic and brain

81 metabolic network alterations that are crucial for predicting the observed nonlinear dose efficacy in clinical
82 studies. Notably, single-daily dosing of LEV may not maintain exposure levels, and could result in
83 elevated C_{min}/C_{max} ratios, thus reducing drug effectiveness and potentially resulting in C_{max} dependent
84 toxicities.

85 Although the precise mechanism of action of LEV in AD is not fully understood, it is known to
86 modulate the release of synaptic neurotransmitters by antagonizing SV2A receptors [8, 15]. Moreover,
87 neuromodulation is thought to occur through the inhibition of presynaptic calcium channels, reducing
88 impulse conductivity and thus enhancing the preferential transmission of low-frequency signals [16].
89 During the repurposing of LEV for use in mild cognitive impairment (MCI) studies, a nonlinear dose-
90 dependent response curve was observed in the form of an inverted paraboloid [17-20]. A study with
91 control and MCI participants imaged with functional magnetic resonance imaging (MRI) while performing
92 a memory task revealed that the low (62.5 mg twice daily (BID)) and moderate (125 mg BID) doses of
93 LEV restored normal hippocampal activity in the dentate gyrus and CA3 regions. However, this
94 effectiveness was not observed in the highest (250 mg BID) dose studied, suggesting a resurgence in
95 nonequilibrium synchronization in the hippocampus [18].

96 Previous work from our lab has explored the pharmacokinetic (PK) and pharmacodynamic (PD)
97 relationships of LEV in a mouse model of AD that could be used to better predict clinical efficacy [21].
98 We evaluated LEV using the validated pipeline of the Model Organism Development and Evaluation for
99 Late Onset Alzheimer's Disease (MODEL-AD) Preclinical Testing Core (PTC), where we determined the
100 PK of LEV in the 5XFAD mouse model, permitting the determination of dose, frequency, and duration for
101 chronic studies. We performed PD assessment followed chronic administration, where ^{18}F -AV45 and ^{18}F -
102 FDG PET/MRI showed dose-dependent reduction in amyloid deposition and glucose uptake across
103 imaging cohorts. Additional sex and dose dependencies were seen in nanoString estimates of
104 transcriptional changes, which underpin the PD changes. Though these results showed significant
105 alterations in PK and PD as a function of treatment, methods to elucidate how LEV modified gene and
106 associated brain networks and how this related to blood and brain drug concentrations (i.e. PK/PD) was
107 not investigated [21].

108 Recent work from our group has applied a metabolic network covariance modeling approach in
109 the 5XFAD model across lifespan (i.e. 4, 6, and 12 mos) [22]. This work permits the interrogation of
110 network changes at the whole brain and sub-network levels, allowing greater insights into the network
111 changes that occur with disease progression. Here, we applied this method to investigate LEV treatment
112 and subsequent interregional metabolic changes in 5XFAD mice of both sexes. Our goal was to establish
113 a clear dose/concentration-dependent relationship of LEV treatment in conjunction with alterations in
114 brain metabolic uptake network and gene expression to better predict clinical efficacy, which is not
115 currently possible using traditional analytical approaches.

116

117 **METHODS**

118 All studies adhered to the ARRIVE guidelines and received approval from the Institutional Animal Use
119 and Care Committees (IACUC at their respective locations).

120

121 *Housing conditions and cohort generation at Indiana University (IU):*

122 Adult male 5XFAD mice, female 5XFAD mice, and non-transgenic WT controls were produced through
123 a breeding program at Indiana University (IU). This involved mating male 5XFAD mice (JAX MMRRC
124 stock #:34848) with female C57BL6/J mice (JAX MMRRC stock #:000664). The animals were
125 accommodated in cages, with up to five mice per cage, and were provided with SaniChip bedding.
126 Throughout the dosing studies, the mice continued to reside in group housing arrangements. The colony
127 room maintained a 12:12 Light:Dark schedule, with lights turning on at 6:00 am. One cohort was studied,
128 designed for the endpoint of ¹⁸F-FDG PET.

129

130 *Housing conditions and cohort generation at The Jackson Laboratory (JAX):*

131 Adult male 5XFAD mice, female 5XFAD mice, and non-transgenic WT controls were bred at JAX using
132 the same breeding methods as those employed at IU. Initially, mice were accommodated in duplex cages
133 with pine bedding, allowing up to five mice per side. The colony room adhered to a 12:12 Light:Dark
134 schedule. For chronic dosing studies, each treatment group consisted of approximately 10-15 mice per

135 sex. To ensure randomization, both treatment and sex were randomized across two cohorts, which were
136 staggered by a 4-week interval. Each cohort was comprised of 5-8 mice per sex per treatment. One week
137 prior to the beginning of the study, the mice were individually housed and subsequently transported to a
138 colony room located adjacent to the behavioral testing facility.

139

140 *Levetiracetam Pharmacokinetic Studies:*

141 *In vivo* PK sampling for LEV was initially carried out at JAX following dosing and serial sampling in 6-
142 month-old male and female 5XFAD mice. LEV (Sigma # L8668-100mg; Lot # 051M4742V) was dissolved
143 in sterile saline (vehicle). Mice (with n=3 dose per sex) were administered doses of 10, 30, and 100 mg/kg
144 (dose volume 10 mL/kg). Serial plasma samples were collected via the tail vein prior to dosing and at
145 0.25, 0.5, 1, 2, 4, 6, and 24 hours post-dosing. Mice were euthanized at 24 hours, brains excised, frozen
146 using dry ice, and stored at -80°C. Samples were shipped to IU for quantification of LEV and PK analysis
147 per our previous work [21].

148

149 *Levetiracetam Quantification:*

150 LEV and etiracetam (ECA) concentrations were determined in plasma and brain samples using
151 LC/MS/MS, with temazepam as an internal standard as described previously [21]. Standard curves were
152 established over a concentration range of 0.3-30000 ng/mL for plasma samples and 0.8-800 ng/g for
153 brain homogenate samples. The inter-day precision ranged from 5.3% to 15.4% for LEV and 10.7% to
154 17.0% for ECA, while the inter-day accuracy ranged from 88.1% to 108.0% for LEV and 88.4% to 103.0%
155 for ECA.

156

157 *Pharmacokinetic Modeling:*

158 PK parameters were initially calculated using standard noncompartmental analysis (NCA) performed with
159 WinNonlin (Phoenix 64, build 8.0.0.3176), as we have previously described [21]. To estimate chronic
160 exposure, a population pharmacokinetic analysis was conducted in Monolix 2023R1 (Lixoft). Apparent
161 clearance (CL/F) and volume (V/F) were allometrically scaled to weight with fixed coefficients of 0.75 and

162 1.0, respectively. Dose and sex were tested as covariates on CL/F and V/F. Model and covariate
163 selection was based on reduction of objective function value of at least 3.84 (χ^2 , $p<0.05$), goodness of fit
164 plots, covariate vs. eta plots, and visual predictive checks. Clearance for individual mice following chronic
165 treatment with levetiracetam was calculated in Sumlx (2023R1, Lixoft) population estimates (thetas), and
166 area under the concentration time (AUC) calculated as dose-normalized clearance. Data were analyzed
167 and plotted in R version 4.3.0 [23].

168

169 *Magnetic Resonance Imaging*

170 High-contrast gray matter images were acquired 2 days prior to PET imaging, where mice were induced
171 with 5% isoflurane in medical oxygen, placed on the head coil, and anesthesia was maintained with 1–
172 3% isoflurane for scan duration. High-resolution T2-weighted (T2W) MRI images were acquired using a
173 3T Siemens Prisma clinical MRI scanner outfitted with a dedicated 4-channel mouse head coil and bed
174 system (RAPID MR, Columbus, OH, United States) per our previous work [21, 25].

175

176 *In vivo PET Imaging and Analysis*

177 Regional brain glycolytic metabolism was monitored using 2-¹⁸F-fluoro-2-deoxy-d-glucose (¹⁸F-FDG),
178 where clinical unit doses ranging from 185 MBq (5 mCi) were purchased from PETNet Indiana (PETNET
179 Solutions Inc.). In all cases, mice were fasted for a minimum of 12 h prior to tracer administration. Mice
180 were injected IP with 3.7–11.1 MBq (100–300 uCi) with ¹⁸F-FDG and allowed 30 min of uptake in an
181 isothermal cage. For imaging, mice were then anesthetized with 5% isoflurane gas and maintained at
182 with 1–3% isoflurane per our previous work [21, 25], and scanned on the IndyPET3 (Rouzes et al., 2004)
183 scanner for 15 min. Images were calibrated, and decay- and scatter-corrected PET images were
184 reconstructed into a single-static image volume according to our previous work [21, 25]. All images were
185 co-registered using a rigid-body mutual information-based normalized entropy algorithm with 9° of
186 freedom and mapped to stereotactic mouse brain coordinates according to our previous work [21, 25].
187 Post-registration, 56 regions were extracted via Paxinos and Franklin's 2007 brain atlas and averaged to
188 yield 28 bilateral regions [26]. Standardized Uptake Value Ratios (SUVr; normalized to cerebellum) were

189 computed for all regions relative to cerebellum, and principal component analysis was performed to
190 provide data reduction for all PET regions. Consensus regions which explained 80% of the variance
191 observed across all regions studied were selected for regional interrogation via MANOVA, correcting for
192 multiple comparisons with a Bonferroni correction. To assess whole brain and sub-network changes in
193 ¹⁸F-FDG images, metabolic covariance analysis was conducted according to our recent work and open
194 source tools [22]. Pearson's correlation between z-scores of region pairs was calculated for all pairwise
195 interactions within each cohort to generate a covariance adjacency matrix (see Figures. 3, 5-7). To
196 assess metabolic network characteristics, a correlation threshold of $p < 0.05$ was applied to adjacency
197 matrices, with only significant edges surviving (Figure 3). Multiple alpha values were tested, but
198 thresholds more restrictive than $p < 0.05$ yielded graphs too sparse for meaningful analysis. The nodal
199 degree, positive strength, negative strength, and clustering coefficient was computed for every brain
200 region and the global distribution of nodal characteristics were compared across sex and treatment using
201 2-sample Kolmogorov-Smirnov (KS) tests. To evaluate the sub-network modules, littermate control (WT)
202 community partitions were generated via multi-resolution consensus clustering (MRCC) analysis [27] and
203 imposed on comparison groups. In sex comparisons, male littermate control partitions were used. Mean
204 metabolic SUVR were compared between like communities via ANOVA, with a Bonferroni correction.
205

206 *Drug Administration for Chronic Studies:*

207 Mice were weighed daily and received oral gavage of LEV (SelleckChem # S1356, bulk lot # S135602)
208 dissolved in sterile saline twice daily (BID) for 3 months. LEV was administered between 7:00 am – 9:00
209 am and 3:00 pm – 5:00 pm, with a dose volume of 10 mL/kg. In all cases, LEV was formulated in sterile
210 saline weekly, and vials were blinded (i.e. A, B, C, and D (JAX) or Blue, Red, Yellow, and Green (IU)) in
211 accordance with ARRIVE guidelines [28]. Drug stability was determined by IU Clinical Pharmacology
212 Analytical Core (CPAC) and was shown to be stable in the final formulation for a one-week period.
213 Throughout the chronic dosing period, animals were closely monitored for potential signs of toxicity or
214 drug-related side effects, where the attrition was very low ($n = 3$). This was not specific to a dose level
215 and occurred either due to dermatitis or lung puncture during oral gavage.

216

217 *Terminal Tissue Collection:*

218 Upon study completion plasma and brain tissue samples were collected from the subjects under
219 isoflurane anesthesia 30 min after the final LEV dose. Bioanalytical analysis was conducted via CPAC
220 for terminal plasma and the right brain hemisphere to confirm PK data. For transcriptional profiling,
221 homogenates from the left hemispheres were quantified using a customized nanoString nCounter®
222 Mouse AD panel designed to identify changes in gene expression associated with clinical LOAD.
223 Differential gene expression was assessed with consideration of genotype, sex, and treatment per our
224 previous work [21].

225

226 *nanoString Gene Expression Profiling and Analysis*

227 Methods for this assay have been published previously [21]. Data were analyzed with the use of QIAGEN
228 IPA (QIAGEN Inc., <https://digitalinsights.qiagen.com/IPA>).

229

230 *Rigor and Reproducibility:*

231 During study execution and throughout data analysis, all technicians adhered to the ARRIVE guidelines
232 [28] and were unaware of the genotype and drug dosage information.

233

234 **RESULTS**

235 *Population Pharmacokinetics*

236 LEV concentration-time data fit a 1-compartment first order absorption model (Figure 1). After accounting
237 for weight, dose (but not sex) was found to be a significant covariate on oral clearance (CL/F) and

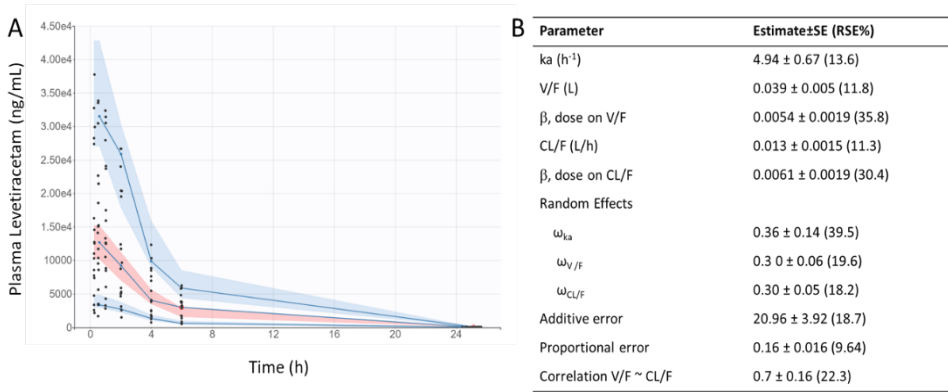


Figure 1. Levetiracetam pharmacokinetics: (A) Visual predictive check demonstrates reasonable fit of population pharmacokinetic model to data. Points indicate individual observed data, solid lines represent median, 5th, and 95th percentiles of observed data, pink shaded area indicates 90% prediction interval of the median, blue shaded areas indicated 90% prediction intervals of the 5th and 95th percentiles of predicted data. (Table 1). Final pharmacokinetic parameter estimates for population model of levetiracetam.

238 apparent volume of distribution (V/F), as indicated by reduced objective function value and improved
 239 covariate vs. η plots. As shown in **Figure 1B**, the predicted AUCs were significantly correlated with 0.5
 240 hour plasma concentrations following twice-daily dosing of levetiracetam in mice housed at JAX ($p < 0.001$,
 241 $R^2 = 0.71$)

242

243 *General Linear Modeling of Brain ¹⁸F-FDG PET*

244 In chronic LEV-treated 5XFAD mice of both sexes, quantitative analysis of ¹⁸F-FDG PET uptake across
 245 different dosage levels was performed after normalizing regional data with a standard uptake value ratio
 246 (SUV_r) to the cerebellum [21, 25]. Using principal component analysis (PCA), twelve out of the twenty-
 247 seven studied regions that consistently explained 80% of the variance in ¹⁸F-FDG uptake between and

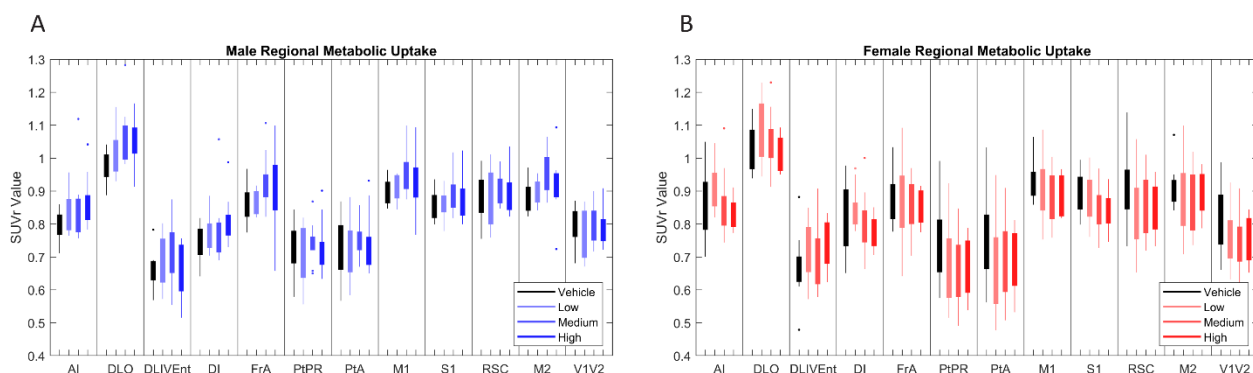


Figure 2: ^{[18}F]-FDG PET standardized uptake value ratio (SUV_r) to cerebellum in brain regions in (A) male and (B) female mice. Principal component analysis (PCA) found that the twelve brain regions above most consistently accounted for 80% of variance in cerebral metabolic uptake across cohorts. Full names of annotated brain region labels can be found in Supplementary Table 1.

within cohorts were identified (see Figure 2). In this model system, dynamic range was determined to have a 1.5-fold difference in ^{18}F -FDG uptake between WT and 5XFAD mice [25], thus supporting its use

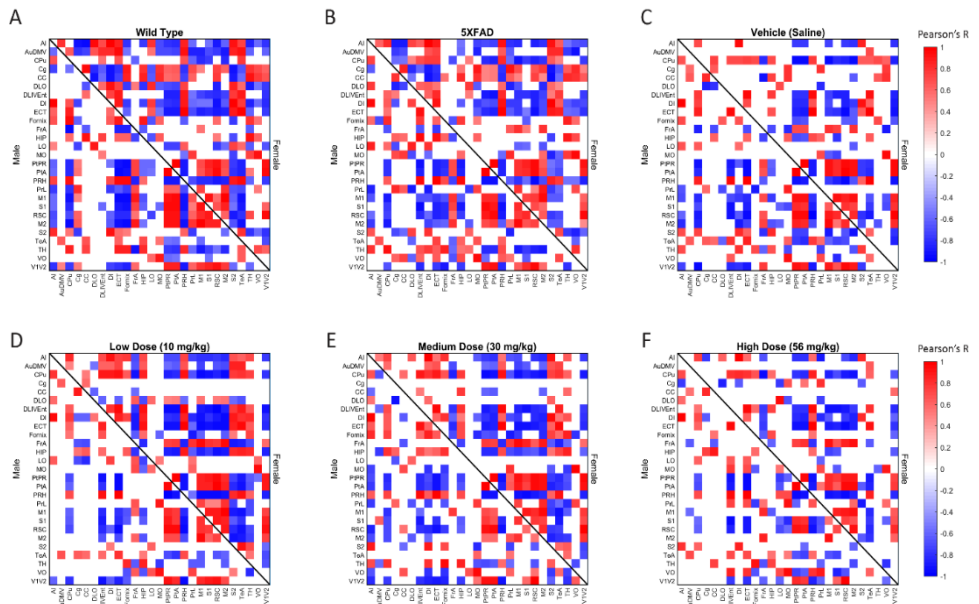


Figure 3: Thresholded metabolic covariance matrices sorted alphabetically by region. Edges were thresholded based on correlation magnitude, with surviving edges having a correlation significance value of $p < 0.05$.

250 for drug discovery studies. Significance was seen at the brain region level across treatments [21], but
251 pairwise interregional interactions were not explained by per-region significance, so a network approach
252 [22, 27, 29] was applied to further investigate interregional metabolic alterations.

253

254 *Global Network Properties*

To measure metabolic changes at a network level, we utilized covariance and connectomic analyses [22, 27, 29]. First, we measured the degree of functional metabolic connectivity on a single-region basis, and extrapolated nodal degree values to a global distribution. For female mice, the network degree of vehicle dose and low dose ($p<0.001$), vehicle dose and medium dose ($p<0.05$), medium dose and high dose ($p<0.01$), and low dose and high dose ($p<0.001$) were significantly different. Interestingly, the vehicle dose and high dose had almost the same network distribution for degree ($p=0.994$), consistent with the findings of previous literature [6]. By contrast, male mice did not follow the same degree changes observed in females, with no two distributions significantly different from one another between treatments (Figure 4A). Qualitatively, we see different connectivity patterns between sexes as a function of

264

treatment. Males displayed oscillatory behavior in degree distributions, with the vehicle group more

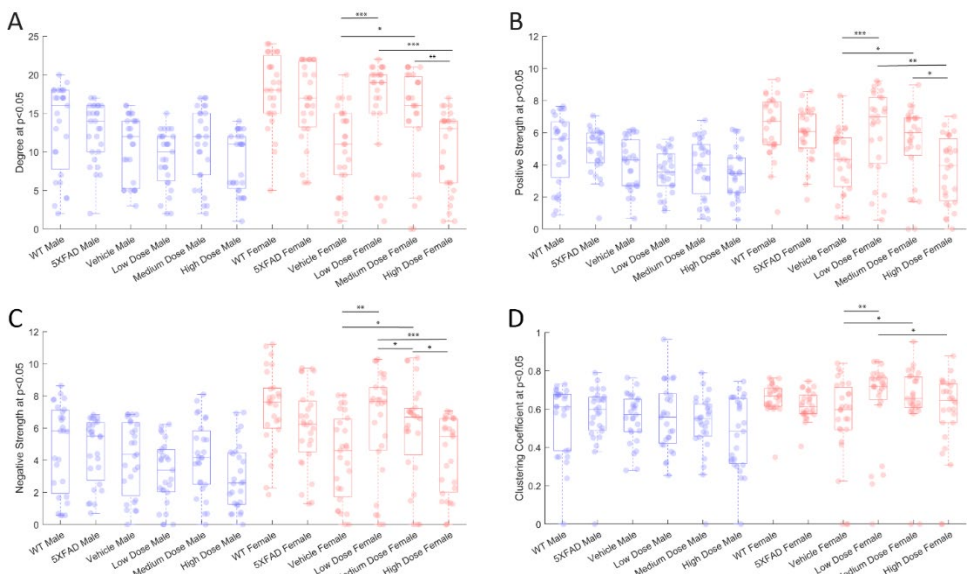


Figure 4: Properties of $p<0.05$ thresholded metabolic covariance for control and treatment groups. (A) Network degree, (B) positive strength, (C) negative strength, and (D) clustering coefficient. * denotes $p < 0.05$, ** denotes $p<0.01$, *** denotes $p<0.005$, 2-sample Kolmogorov-Smirnov test significance.

265

connected than low and high doses, but less connected than medium dose. By contrast, female mice
266 showed a clear dose-dependent change in degree of connections, with the networks of low and medium
267 dosed mice significantly more connected than those of the vehicle and high dosed mice. To look further
268 into the weight and sign of functional connections between regions, we analyzed the positive and
269 negative weighted node degree of every region in the brain, known and positive and negative strength,
270 respectively. In females, the distributions of positive node strengths across the brain after a $p<0.05$
271 threshold was applied significantly differed between vehicle and low dose ($p<0.001$), vehicle and medium
272 dose ($p<0.05$), medium and high dose ($p<0.01$), and low and high dose ($p<0.01$). Negative strengths in
273 females resembled positive strengths in their distributions across treatment, both qualitatively in the same
274 inverted paraboloid shape (see Figure 4B,C), and quantitatively with significant differences between the
275 same groups as positive strengths, with the addition of significance between low and medium dose
276 ($p<0.05$) not seen in positive strengths. Males did not show any significant differences between
277 distributions of either positive or negative strengths after a $p<0.05$ threshold was applied to the covariance
278 matrix. To measure the functional interconnectivity of brain subnetworks, clustering coefficients
279 (propensity of connected triangles in a network) were calculated and compared in the same manner as
280 the prior network characteristics. The clustering coefficients of brain networks followed a similar pattern

281 across treatment for each sex. Significance was seen in the distribution of clustering coefficient in female
282 networks between vehicle dose and low dose ($p<0.01$), vehicle dose and medium dose ($p<0.05$) and low

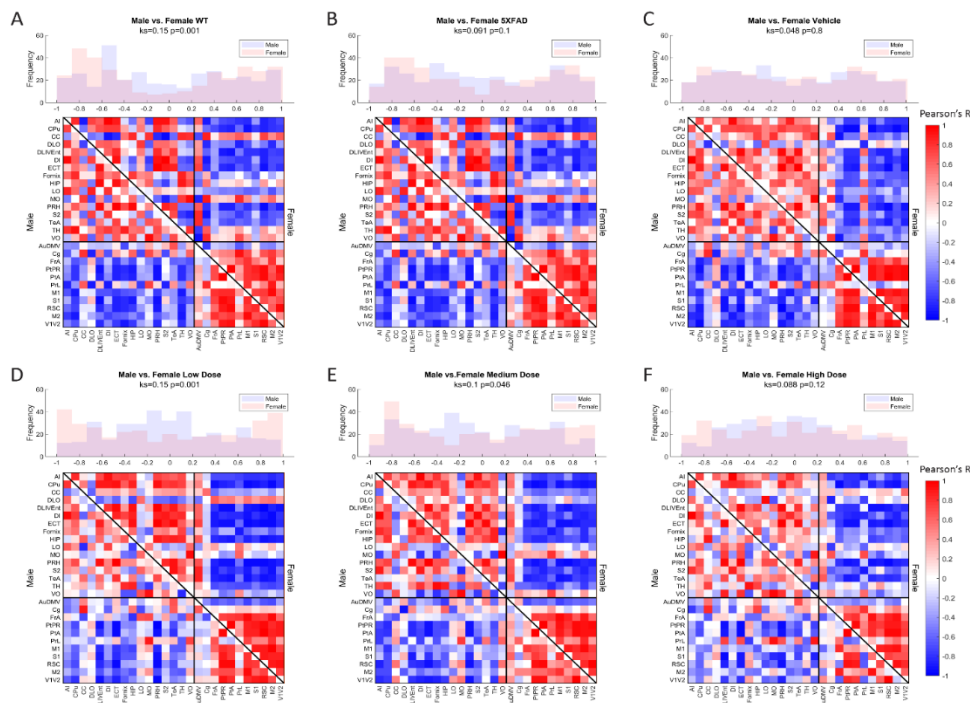


Figure 5: Metabolic ($[^{18}\text{F}]\text{-FDG}$) covariance matrices for (A) wild-type (WT), (B) 5XFAD, and (C-F) treatment groups with male WT community partitions applied on upper (female) and lower (male) triangles. Histograms of interregional correlation values indicate correlation distribution across all brain regions for each respective cohort. Covariance was computed as Pearson's correlation of z-scored regional SUVR values across animals within each group. Distributions between sexes of a given cohort are compared with a 2-sample Kolmogorov-Smirnov (KS) nonparametric test, with KS-value and p-value printed above the histogram.

283 dose and high dose ($p<0.05$), while males did not show significant differences that survived the $p<0.05$
284 threshold.

285

286 *Effect of Treatment on Covariance Distributions*

287 Distributions of Pearson's correlation between regions denoted by edge weight differed across sex and
288 treatment, as measured by a two-sample KS non-parametric distribution comparison (see Figures 5-7).
289 Males exhibited little handling stress, with qualitatively similar partitioned adjacency and edgewise
290 distribution between 5XFAD disease control and saline-dosed vehicle cohorts (Figure 6B). Males treated
291 chronically with a low dose (10 mg/kg) of LEV yielded a more normally distributed set of edgewise
292 covariance trending towards significance compared to the vehicle (saline) treatment group of the same

293 sex (KS = 0.01, $p = 0.057$). By contrast, males treated with the high dose (56 mg/kg) of LEV yielded a
294 covariance distribution significantly different from the vehicle treated group (KS = 0.12, $p < 0.05$) (Figure
295 5E). Unlike males, females exhibited relationships in ^{18}F -FDG covariance between treatments in the
296 medium (30 mg/kg) and high (56 mg/kg) doses groups which trended towards significance (Figure 7D,E).
297 Importantly, there was a significant sex effect with treatment distributions, where male and female cohorts
298 were significantly different between low (KS = 0.15, $p < 0.005$) and medium (KS = 0.1, $p < 0.05$) dose,
299 with males qualitatively more normally distributed than females (Figure 5).

300

301 *Community Structure and Component Function with Sex*

302 Metabolic covariance networks were assessed via the MRCC community detection algorithm with 10,000
303 permutations to establish a rigorous partition for covariance networks focused on positive covariance
304 between regions [22, 29] where partitions, or communities, differed between sexes and treatments.
305 Female modularity ranged from two to five communities within a network, with the number of partitions
306 generally increasing linearly as a function of dose. Male modularity consistently had more partitions
307 relative to females, with the lowest number of modules present in the low dose group and an average of
308 5.66 modules across other treatments. We interpreted the number of communities as indicative of
309 edgewise coherence among regions, akin to functional subnetworks. We observe that males generally
310 exhibit a greater number of subnetworks relative to females. This agrees with our findings from the
311 observations of node degree and strength distributions. Males form subnetworks of highly similar
312 metabolic covariance, while the most similar partition structure for females tends towards large,
313 bidirectional networks, consistent with higher degrees of connectivity across regions relative to males
314 across treatments groups. To track network changes in a common reference space, we imposed the
315 community structure of the healthy control WT male metabolic covariance network onto male and female

316 network of the same treatment across all treatments (Figure 5). Male littermate controls were chosen as
 317 the reference network partition due to consensus findings of females displaying more aggressive AD
 318 disease phenotype at a given age, both in the 5XFAD model and in human AD pathology [25]. Using
 319 male littermate controls therefore enabled better tracking of deviations from a healthy metabolic network.

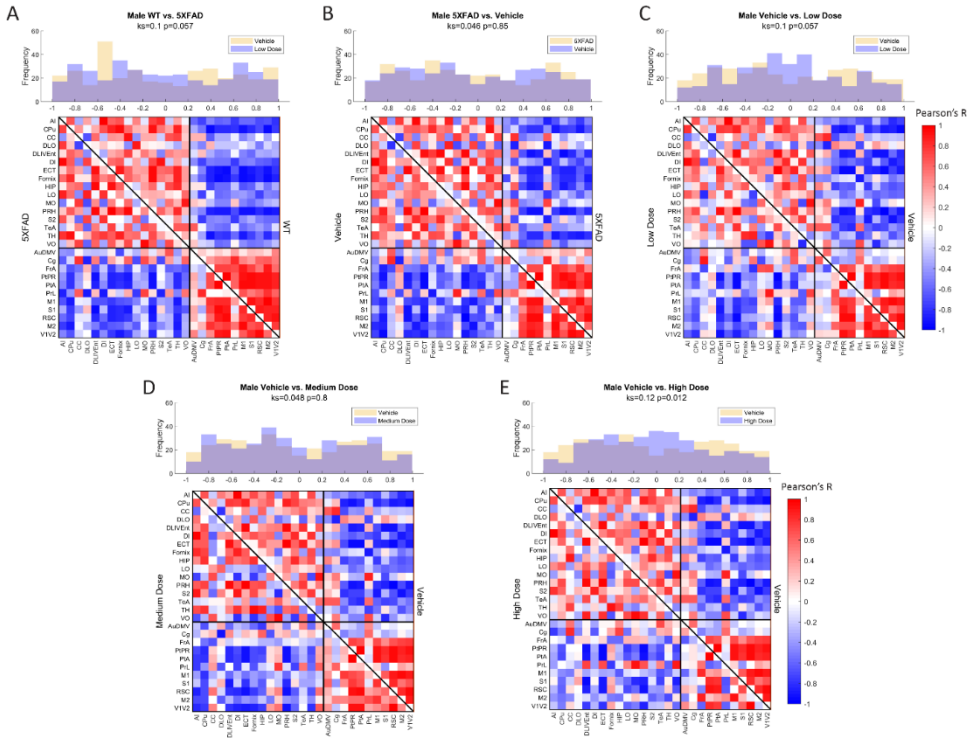


Figure 6: Male metabolic covariance matrices across treatment with WT community partitions applied. Changes in functional network structure can be observed via (A) changes in network and covariance distribution due to disease, (B) handling stress, and (C-E) dose difference.

320 To assess differences in metabolic uptake distributions in subnetworks between males and females at a
 321 given treatment, we performed ANOVA between male and female metabolic SUVR networks clustered by
 322 WT male MRCC partitions. Significance was corrected for multiple comparisons via Bonferroni correction.
 323 We found that at vehicle, low, and high dose, there were no significant differences in metabolic uptake in
 324 communities of the same regional groupings between sexes; however, at low dose, of the two
 325 communities detected in the male MRCC algorithm, one yielded significantly different metabolic uptake.
 326 The first community was composed of the following region members: AI, CPu, CC, DLO, DLIVEnt, DI,
 327 ECT, Fornix, HIP, LO, MO, PRH, S2, TeA, TH, and VO (See Supplemental Table 1 for full region names).
 328 At low dose, females exhibited significantly more uptake in this subnetwork than males ($F = 4.9$, $p < 0.05$).

329 The functional interpretation of this subnetwork, using equally weighted components, was determined to
330 be primarily learning, with additional components of perception and sensory processing. Within sex,
331 males displayed significantly different metabolic uptake between vehicle and medium dose in the

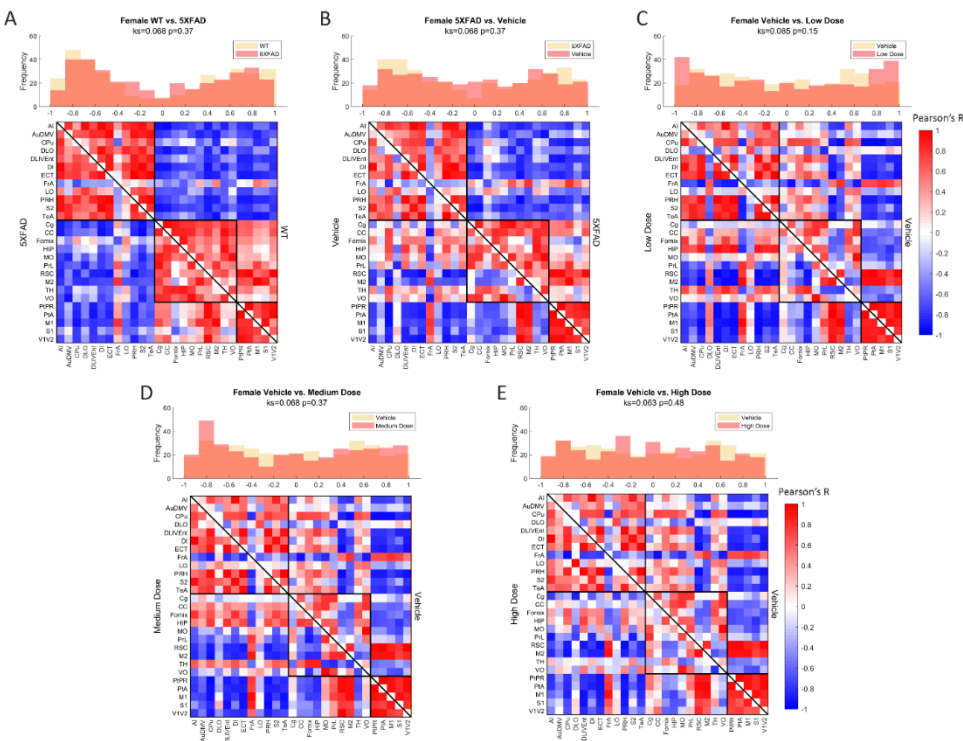


Figure 7: Female metabolic covariance matrices across treatment with WT community partitions applied. Changes in functional network structure can be observed via (A) changes in network and covariance distribution due to disease, (B) handling stress, and (C-E) dose difference.

332 subnetwork containing AuDMV, Cg, FrA, PtPR, PtA, PrL, M1, S1, RSC, M2, and V1V2 ($F = 4.7$, $p < 0.05$).
333 Functionally, the regions within this subnetwork encoded primarily for learning and sensory processing.
334 Females did not display significantly different uptake in common communities between treatments.

335

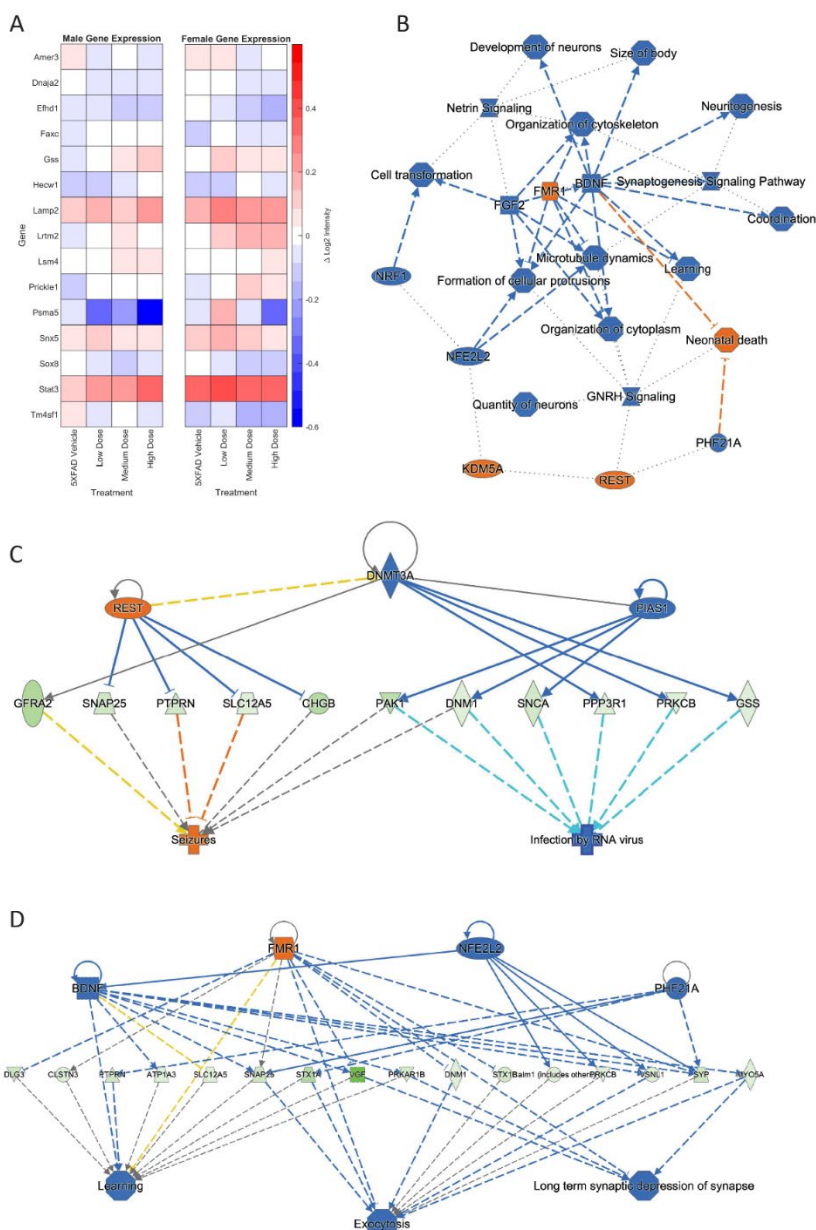


Figure 8: (A) Log2 intensity gene expression difference in male and female 5XFAD treatment groups from male and female WT vehicle groups, respectively. Gene expression at treatment level was subtracted from expression at vehicle, and results plotted as a heat map. Genes plotted are linked to AD, epileptiform activity, cerebral metabolism, and/or cerebral homeostatic mechanisms. (B) Primary GO pathway analysis found the processes connected to similarly expressed genes between medium and high dosed female mice. Further pathway analysis focused found connections to (C) seizure, (D) learning, exocytosis, and long-term depression functions. See Supplementary figure 1 for prediction legend.

Brain hemispheres were assessed via nanoString for gene expression differences using a panel

based on human AD gene expression changes [30-34]. Linear regression analysis revealed 15 genes

that were significant at $p < 0.05$ for genotype, sex, and/or treatment. As shown in Figure 8A, the change

in log₂ intensities from WT vehicle mice demonstrated undirected significant dose-specific effects for

341 genes which encode for AD, epileptiform activity, cerebral metabolism, and/or cerebral homeostatic
342 mechanisms. Further analyses were performed on genes from medium and high dose treated animals
343 that were significantly anti-correlated with neuronal-related human modules in the inferior frontal gyrus
344 (IFG) region [34]. This gene module identified 129 genes, and Gene ontology (GO) enrichment analysis
345 identified a number of biological processes, which, consistent with the mechanism of action of LEV [35],
346 included synaptic vesicle cycling, vesicle exocytosis, vesicle recycling, vesicle priming, regulated
347 exocytosis, neurotransmitter transport, neurotransmitter secretion, and protein localization to cellular
348 junctions [21, 34] (see Figure 8B). Further pathway analyses performed on these 129 genes with
349 Ingenuity Pathway Analysis (IPA) [36] revealed significant overlap with canonical pathways ‘SNARE
350 signaling pathway’, ‘Netrin Signaling’, ‘Synaptogenesis signaling pathway’, ‘mitochondrial dysfunction’
351 and ‘Glutaminergic Receptor Signaling pathway (enhanced)’. Top regulator effect networks were also
352 identified, such as’ ‘Exocytosis and Learning’ comprised of *BDNF*, *FMR1*, *NFE2L2* and *PHF21A*, and
353 ‘Seizures’ comprised of *DNMT3A*, *PIAS1* and *REST*. Lastly, ‘memantine’ was determined to be both a
354 significant upstream regulator and driver of the causal network. Memantine [24], also known as
355 Namenda, was one of the first approved drugs to treat AD and has a similar target to LEV: it works as an
356 NMDA receptor antagonist aimed at quelling abnormal activity in the brain. Overall, identification of
357 specific processes and pathways relevant to drug treatment help to narrow mechanisms and refine
358 preclinical translation from mouse to human studies.

359

360 *Exposure-Response Modeling*

361 Despite the plasma concentration AUC relationship and the dose dependent changes observed with
362 metabolic connectomics, no apparent relationships could be established with connectomics data when
363 PK/PD modelled using a multi-linear regression. By contrast, expression changes in Amer3, Lamp2,

364 Lrtm2, Psma5, and Stat3 all showed significant associations ($p < 0.05$) with LEV concentration and/or

| | AUC $\beta \pm SE$ (p-value) | Sex $\beta \pm SE$ (p-value) | R^2 |
|-------|-------------------------------|------------------------------|-------|
| Amer3 | -0.006 \pm 0.0003 (0.024) | 0.014 \pm 0.021 (0.5) | 0.04 |
| Lamp2 | 0.00075 \pm 0.0002 (0.0013) | -0.069 \pm 0.017 (<0.001) | 0.21 |
| Lrtm2 | 0.00098 \pm 0.00046 (0.04) | -0.085 \pm 0.035 (0.02) | 0.078 |
| Psma5 | -0.0036 \pm 0.0017 (0.04) | -0.0016 \pm 0.13 (0.99) | 0.025 |
| Stat3 | 0.001 \pm 0.0004 (0.16) | -0.11 \pm 0.03 (<0.001) | 0.16 |

Table 2. Association between gene expression and levetiracetam exposure (AUC) and Sex. Modelling was calculated in R using lm(Y~AUC + SEX)

365 animal sex (Table 2, Figure 9).

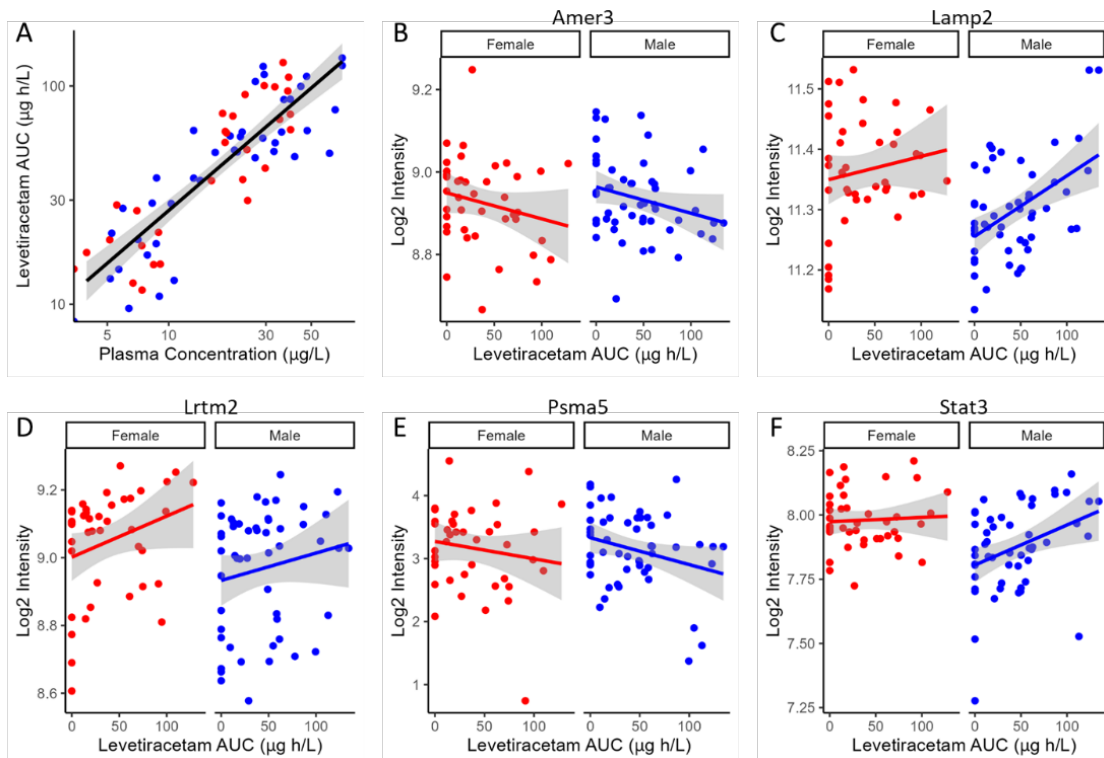


Figure 9: (A) Levetiracetam exposure (AUC) as a function of plasma concentration with a linear regression applied and 95% confidence interval plotted. Gene expression in terms of Log2 intensity is plotted as a function of AUC for the five genes (B-F) which showed significant sex dependency.

366 **DISCUSSION**

367 In the current study, we performed retrospective network analysis of LEV data to gain novel insight
 368 about how chronic dosing affects AD progression as it pertains to cerebral metabolic uptake and gene
 369 expression. Our results show that 6-month-old 5XFAD mice display significant changes in metabolic
 370 uptake as seen by network analyses correlated within and between regions in both sexes and across

371 treatment. Per previous studies, we conducted general linear statistical modeling of regional ^{18}F -FDG
372 uptake data as a measure of regional brain function. Quantitative analysis of these data revealed a sex-
373 by-dose relationship [21]; however, due to limitations of these approaches, post-hoc analysis only
374 permitted pair-wise analysis of regional data, thus negating the inter-regional network changes that
375 support higher brain function [22]. To overcome this, we applied network covariance analysis to ^{18}F -FDG
376 data, which has been shown to distinguish stage of disease for both preclinical [22] and clinical AD [29].
377 Using this approach, we quantified pairwise network covariance for all regions, then computed edgewise
378 network features by calculating distributions of degree, positive and negative strength, and clustering
379 coefficient in metabolic networks from thresholded networks. We extrapolated per-region node
380 characteristics to global distributions and compared changes in distributions between treatment within
381 sex. At 6 months, female mice displayed significantly more interregional metabolic uptake as seen by the
382 degree and density of both diseased mice and their littermate controls (Figure 4). Overall, network
383 characteristics indicated that the magnitude of interregional metabolic correlation decreased as chronic
384 dose concentration increased in males, as seen in global degree, and strength outputs. In females,
385 disease and handling stress decreased interregional functional connectivity, some of which was
386 recovered in a dose-dependent manner. Females dosed chronically at 10 mg/kg showed the greatest
387 metabolic network change across analyses, consistent with the mode of action of LEV. More generally,
388 network alteration was inversely proportional to dose concentration in females (Figure 4).

389 Differences in uptake in control cohorts were not localized to specific communities between sexes
390 in 5XFAD mice when the male community partition was applied to both groups, but differences were
391 localized to module 1 of the male partition structure in WT mice ($p<0.05$, Bonferroni corrected). While
392 vehicle, medium, and high doses did not exhibit significantly different uptake between like communities,
393 low dose male and female mice exhibited significant differences in metabolic uptake in one of two
394 modules. Based on the region members of this module, these changes are expected to impact learning,
395 memory, and sensory integration, and are consistent with LEV mode of action.

396 5XFAD is known to be an aggressive amyloidogenic early-onset model of Alzheimer's disease.
397 Like AD, 5XFAD mice exhibit sexual dimorphism in pathology, with females displaying a more rapid onset

398 disease phenotype [25]. Previous studies have presented conflicting findings on cerebral metabolic
399 uptake in the 5XFAD model around 6 months [25]. In the current study, we treat littermate controls as a
400 reference population and explore the changes of metabolic networks with respect to littermate controls.
401 We hypothesized that within sex, we would see a dose-dependent response evident in network
402 characteristics and community structure. We also hypothesized that this dose-dependency would vary
403 between sexes, with females showing a greater restorative response in part due to their faster
404 progression towards disease state.

405 Comparing littermate controls to diseased (5XFAD) mice, there were surprisingly few differences
406 in male and female adjacency matrices when community partition structure of their WT littermates was
407 applied. By contrast, female 5XFAD mice exhibited a greater handling stress response than males, and
408 this stress response was localized to interregional correlation shifts in the retrosplenial cortex (RSC) and
409 secondary motor cortex (M2). This is consistent with amyloid deposition previously reported for these
410 structures [25]. This handling effect was observed in all female LEV dosed cohorts (see Figure 7B-E). At
411 low dose, neither females nor males had network alterations significantly different from vehicle, though
412 males trended towards significance. At medium dose, females showed qualitative differences in network
413 structure compared to vehicle in the interregional correlations of the frontal association cortex as well as
414 the lateral orbitofrontal cortex. Males showed similar qualitative differences in lateral orbitofrontal
415 correlations, but neither sex differed from vehicle at the medium dose. At high dose, males significantly
416 differed from vehicle in edgewise correlations with many weak correlations relative to vehicle ($p<0.05$)
417 (Figure 6E). Females, on the other hand, did not display significant edgewise distributions, and instead
418 converged back towards vehicle distribution relative to medium and low dose. This finding is consistent
419 with dose-dependent findings of previous LEV studies [21]; at high chronic doses of LEV, females both
420 in mice as well as in the clinic develop a functional resistance to the drug, the exact cause of which is yet
421 to be uncovered [10, 21, 37, 38]. WT covariance distributions were significantly different between males
422 and females ($p<0.005$). Females display a greater number of strong correlations, both positive and
423 negative, between regions. This is consistent with previous literature showing that WT females show
424 marginally greater glycolytic metabolism in the brain after ~6 months of age [25]. 5XFAD mice displayed

425 no significant difference in their distributions, however, females did show a bimodal distribution with the
426 highest frequency of covariance values occurring at the limits. In low and medium doses, female
427 edgewise distributions were again bimodal and significantly different from males ($p<0.005$ and $p<0.05$,
428 respectively). These differences further reinforce the sexual dimorphism of 5XFAD mice which has been
429 previously reported [21, 22, 25, 39], and are thought to be linked to the transgene expression being linked
430 to the estrogen sensitive Thy1 promoter [40].

431 Network analyses of thresholded metabolic correlation networks, like edgewise distributions,
432 revealed network characteristics that differed on a sex by treatment basis. WT mice follow a pattern with
433 females' retaining greater numbers of nodes than their male counterpart, as seen in network degree and
434 clustering coefficient distributions (Figure 3A,D). Vehicle cohorts showed a sex-specific decrease in
435 density relative to WT and likely represents handling stress. This handling stress is consistent with prior
436 findings which show that female mice exhibit higher stress hormone response than their male
437 counterparts when introduced to handling stressors [41]. At low and medium dose, we see network
438 degree approach WT levels only to decline at a high dose of LEV, which we interpreted as due to
439 functional tolerance. Further analysis of positive and negative network strengths support the sex and
440 dose dependency in whole brain networks. Females contain more positive and negative strengths than
441 males at every treatment, and the low and medium LEV doses show a significant increase in positive and
442 negative strengths (Figure 4B,C). This supports the notion that in AD pathology, signal disruption is seen
443 both in suppression of some circuits and aberrant activity of others, resulting in more extreme
444 interregional relationships [6]. Previous studies [7, 10, 21] have reported that LEV reduces sub-seizure
445 epileptiform activity in mouse models of AD [22] and we believe that by reducing aberrant neuronal
446 activity, LEV perturbs hyperactive neural circuitry back towards a functional equilibrium with decreased
447 signal suppression distal to A β plaques and a regulation of aberrant activity near plaques. However,
448 specificity between equilibrium metabolic uptake in neurons, glia, and other energy-demanding cerebral
449 machinery and nonequilibrium inflammation-driven metabolic uptake in microglia and hyperactive
450 dysregulated circuits cannot be distinguished in ^{18}F -FDG PET imaging {Xiang, 2021 #50}. Because of
451 this, we conducted targeted transcriptomic analysis using nanoString to track gene expression and

452 identified fifteen genes to be dose and sex dependent (See Figure 8A). Further analyses examining GO
453 biological processes and pathway overlap in genes shared between medium and high-dosed animals
454 were primarily representative of synaptic function and organization. This was not overly surprising, as the
455 genes analyzed were selected as they were correlated with human AD genes in the Neuronal Consensus
456 cluster. However, this helped to narrow future focus on such pathways as SNARE and glutaminergic
457 signaling which may be important components of LEV signaling.

458 As with all studies, there are limitations that must be considered when drawing conclusions. First,
459 the 5XFAD model was developed as a rapid-onset, highly aggressive representation of early-onset
460 Alzheimer's disease. 5XFAD displays early amyloid beta plaque formation relative to other mouse models
461 and epileptiform activity localized to the dentate gyrus and hippocampus, spatially analogous to human
462 data [42]. However, 5XFAD mice have been shown not to express behavioral disease phenotype relative
463 to controls analogous to MCI and AD patients in the clinic [25]. With this in mind, the current study
464 revealed novel interactions that can provide insight into cerebral metabolic modulation by LEV in AD.
465 LEV clearly acts in a dose and sex-dependent manner, with network alteration relying on the degree of
466 disease phenotype present in the subject. To more completely understand the network effects of LEV,
467 future studies might use less severe, more physiologically analogous mouse models of AD, and bear in
468 mind sexual dimorphism to test LEV efficacy in both sexes at equivalent disease phenotypes. MODEL-
469 AD is currently longitudinally testing novel models of AD which may fulfill these requirements {Oblak,
470 2020 #51}] and studying the effect of LEV on disease progression in these models may be more
471 translationally viable. An additional limitation discussed in the original study is the choice of LEV dose
472 chronically administered to these mice [21]. Future studies looking at LEV's metabolic modulatory effects
473 may choose more intermediate doses than the ones in this study gain a more in-depth understanding of
474 edgewise changes in community structures as well as between regions. Analytical tools to connect
475 regional components of functional metabolic correlation communities to their emergent functional
476 properties such as sensory, motor, or integration hubs are currently in development, and will shed light
477 on the nature of metabolic restructuring in terms of edgewise correlation shifts.

478 Previous studies show that LEV likely acts near circuits or networks plagued by beta amyloid
479 deposition [10, 43]. In the original PTC study, mice underwent ¹⁸F-AV45 PET imaging according to the
480 same protocols of the ¹⁸F-FDG imaging [21]. Future studies utilizing PET imaging of amyloid deposition
481 in mouse models to map the co-localization of this structural network with the functional networks given
482 by metabolic PET imaging may shed more insight into metabolic perturbation of AD pathology with
483 respect to amyloid imaging. Moreover, combining these with transcriptomics and PK/PD modeling could
484 lead to a more precise indication of drug efficacy. This, in turn, would have significant translational
485 implications for precision medicine and treatment of the synchronized hyperactive neural activity seen in
486 patients with AD.

487 In the previous study, gene expression analysis revealed that in an Accelerating Medicines
488 Partnership Program for Alzheimer's Disease (AMP-AD) consensus clusters of genes, females exhibit
489 anticorrelation in gene expression with respect to analogous human expression, suggesting that at high
490 chronic dosing of LEV, there may be effects seen that cannot be explained by our functional tolerance
491 interpretation [21, 30]. Future work may utilize a multimodal approach involving higher throughput and/or
492 spatial transcriptomics coupled with metabolic uptake quantification to better resolve ambiguities in the
493 physiological effects of LEV dose-wise.

494 In conclusion, our research revealed significant dose-dependent changes in region-wise glycolytic
495 correlation and gene expression changes in response to LEV not possible with traditional general linear
496 statistical modeling. Further, it revealed a sex and dose dependency that provides a means to track
497 network changes using translationally relevant ¹⁸F-FDG PET imaging.

498
499 **Data Availability:** All protocols, raw, and summary data are available at <https://adknowledgeportal.org>,
500 where the Synapse ID is syn2580853, and DOI is [10.7303/syn2580853](https://doi.org/10.7303/syn2580853).

501
502 **Acknowledgements:** The authors would like to acknowledge the JAX Center for Biometric Analysis staff
503 for support of the chronic dosing studies. In addition, we would like to acknowledge the JAX Genome
504 Technologies core for assistance with nanoString RNA extractions and sample processing. The current

505 study data, in whole or in part, were obtained from the AD Knowledge Portal
506 (<https://adknowledgeportal.org>), and the brain covariance analysis software was obtained from the
507 publicly available CovNet package (<https://github.com/echumin/CovNet>).

508

509 **Competing Interests:** The authors do not report any competing interests.

510

511 **Funding Sources:** The data for this study were funded through grant NIA [U54AG054345](#).

512

513 **References**

514 1. Vossel, K.A., et al., *Incidence and impact of subclinical epileptiform activity in Alzheimer's*
515 *disease*. Annals of Neurology, 2016. **80**(6): p. 858-870.

516 2. Minkeviciene, R., et al., *Amyloid β -Induced Neuronal Hyperexcitability Triggers*
517 *Progressive Epilepsy*. The Journal of Neuroscience, 2009. **29**(11): p. 3453-3462.

518 3. Angulo, S.L., et al., *Amyloid pathology-produced unexpected modifications of calcium*
519 *homeostasis in hippocampal subiculum dendrites*. Alzheimer's & Dementia, 2020.
520 **16**(2): p. 251-261.

521 4. Stafstrom, C.E., *The role of the subiculum in epilepsy and epileptogenesis*. Epilepsy Curr,
522 2005. **5**(4): p. 121-9.

523 5. Tran, T.T., et al., *Increased hippocampal activation in ApoE-4 carriers and non-carriers*
524 *with amnestic mild cognitive impairment*. Neuroimage Clin, 2017. **13**: p. 237-245.

525 6. Palop, J.J., et al., *Aberrant Excitatory Neuronal Activity and Compensatory Remodeling*
526 *of Inhibitory Hippocampal Circuits in Mouse Models of Alzheimer's Disease*. Neuron,
527 2007. **55**(5): p. 697-711.

528 7. Palop, J.J., *Epilepsy and Cognitive Impairments in Alzheimer Disease*. Archives of
529 Neurology, 2009. **66**(4): p. 435.

530 8. Kumar, A., K. Maini, and R. Kadian, *Levetiracetam*, in *StatPearls*. 2023: Treasure Island
531 (FL).

532 9. Vossel, K., et al., *Effect of Levetiracetam on Cognition in Patients With Alzheimer Disease*
533 *With and Without Epileptiform Activity*. JAMA Neurology, 2021. **78**(11): p. 1345.

534 10. Sanchez, P.E., et al., *Levetiracetam suppresses neuronal network dysfunction and*
535 *reverses synaptic and cognitive deficits in an Alzheimer's disease model*. Proceedings of
536 the National Academy of Sciences, 2012. **109**(42): p. E2895-E2903.

537 11. Lippa, C.F., et al., *Levetiracetam: a practical option for seizure management in elderly*
538 *patients with cognitive impairment*. Am J Alzheimers Dis Other Demen, 2010. **25**(2): p.
539 149-54.

540 12. Toniolo, S., A. Sen, and M. Husain, *Modulation of Brain Hyperexcitability: Potential New*
541 *Therapeutic Approaches in Alzheimer's Disease*. Int J Mol Sci, 2020. **21**(23).

542 13. Klee, J.L., et al., *Reduced firing rates of pyramidal cells in the frontal cortex of APP/PS1*
543 *can be restored by acute treatment with levetiracetam*. Neurobiology of Aging, 2020. **96**:
544 p. 79-86.

545 14. Schneider, F., et al., *Behavioral and EEG changes in male 5xFAD mice*. Physiol Behav,
546 2014. **135**: p. 25-33.

547 15. Lynch, B.A., et al., *The synaptic vesicle protein SV2A is the binding site for the*
548 *antiepileptic drug levetiracetam*. Proceedings of the National Academy of Sciences, 2004.
549 **101**(26): p. 9861-9866.

550 16. García-Pérez, E., et al., *Levetiracetam accelerates the onset of supply rate depression in*
551 *synaptic vesicle trafficking*. Epilepsia, 2015. **56**(4): p. 535-545.

552 17. Bakker, A., et al., *Response of the medial temporal lobe network in amnestic mild*
553 *cognitive impairment to therapeutic intervention assessed by fMRI and memory task*
554 *performance*. Neuroimage-Clinical, 2015. **7**: p. 688-698.

555 18. Bakker, A., et al., *Reduction of Hippocampal Hyperactivity Improves Cognition in*
556 *Amnestic Mild Cognitive Impairment*. Neuron, 2012. **74**(3): p. 467-474.

557 19. Musaeus, C.S., et al., *Levetiracetam Alters Oscillatory Connectivity in Alzheimer's*
558 *Disease*. Journal of Alzheimers Disease, 2017. **58**(4): p. 1065-1076.

559 20. Magalhães, J.C., et al., *The Influence of Levetiracetam in Cognitive Performance in*
560 *Healthy Individuals: Neuropsychological, Behavioral and Electrophysiological Approach*.
561 Clinical Psychopharmacology and Neuroscience, 2015. **13**(1): p. 83-93.

562 21. Onos, K.D., et al., *Pharmacokinetic, pharmacodynamic, and transcriptomic analysis of*
563 *chronic levetiracetam treatment in 5XFAD mice: A MODEL-AD preclinical testing core*
564 *study*. *Alzheimers Dement (N Y)*, 2022. **8**(1): p. e12329.

565 22. Chumin, E., et al., *Brain Metabolic Network Covariance and Aging in a Mouse Model of*
566 *Alzheimer's Disease*. *bioRxiv*, 2023: p. 2023.06.21.545918.

567 23. Team, R.C., *_R: A Language and Environment for Statistical Computing_*. 2023, R
568 Foundation for Statistical Computing: Vienna, Austria.

569 24. Lipton, S.A., *Paradigm shift in neuroprotection by NMDA receptor blockade: memantine*
570 *and beyond*. *Nat Rev Drug Discov*, 2006. **5**(2): p. 160-70.

571 25. Oblak, A.L., et al., *Comprehensive Evaluation of the 5XFAD Mouse Model for Preclinical*
572 *Testing Applications: A MODEL-AD Study*. *Front Aging Neurosci*, 2021. **13**: p. 713726.

573 26. Paxinos, G. and M. Keith B. J. Franklin, *The Mouse Brain in Stereotaxic Coordinates*.
574 2007: Elsevier Science.

575 27. Jeub, L.G.S., O. Sporns, and S. Fortunato, *Multiresolution Consensus Clustering in*
576 *Networks*. *Scientific Reports*, 2018. **8**(1).

577 28. Percie du Sert, N., et al., *Reporting animal research: Explanation and elaboration for the*
578 *ARRIVE guidelines 2.0*. *PLoS Biol*, 2020. **18**(7): p. e3000411.

579 29. Veronese, M., et al., *Covariance statistics and network analysis of brain PET imaging*
580 *studies*. *Scientific Reports*, 2019. **9**(1).

581 30. Preuss, C., et al., *A novel systems biology approach to evaluate mouse models of late-*
582 *onset Alzheimer's disease*. *Mol Neurodegener*, 2020. **15**(1): p. 67.

583 31. Mostafavi, S., et al., *A molecular network of the aging human brain provides insights into*
584 *the pathology and cognitive decline of Alzheimer's disease*. *Nat Neurosci*, 2018. **21**(6): p.
585 811-819.

586 32. Allen, M., et al., *Human whole genome genotype and transcriptome data for Alzheimer's*
587 *and other neurodegenerative diseases*. Sci Data, 2016. **3**: p. 160089.

588 33. Wang, M., et al., *The Mount Sinai cohort of large-scale genomic, transcriptomic and*
589 *proteomic data in Alzheimer's disease*. Scientific Data, 2018. **5**(1): p. 180185.

590 34. Wan, Y.-W., et al., *Meta-Analysis of the Alzheimer's Disease Human Brain Transcriptome*
591 *and Functional Dissection in Mouse Models*. Cell Reports, 2020. **32**(2): p. 107908.

592 35. Dubovsky, S.L., et al., *Levetiracetam, Calcium Antagonism, and Bipolar Disorder*. J Clin
593 Psychopharmacol, 2015. **35**(4): p. 422-7.

594 36. Kramer, A., et al., *Causal analysis approaches in Ingenuity Pathway Analysis*.
595 Bioinformatics, 2014. **30**(4): p. 523-30.

596 37. Surges, R., K.E. Volynski, and M.C. Walker, *Review: Is levetiracetam different from other*
597 *antiepileptic drugs? Levetiracetam and its cellular mechanism of action in epilepsy*
598 *revisited*. Therapeutic Advances in Neurological Disorders, 2008. **1**(1): p. 13-24.

599 38. Löscher, W. and D. Schmidt, *Experimental and Clinical Evidence for Loss of Effect*
600 *(Tolerance) during Prolonged Treatment with Antiepileptic Drugs*. Epilepsia, 2006. **47**(8):
601 p. 1253-1284.

602 39. Jullienne, A., et al., *Cortical cerebrovascular and metabolic perturbations in the 5xFAD*
603 *mouse model of Alzheimer's disease*. Front Aging Neurosci, 2023. **15**: p. 1220036.

604 40. Moechars, D., et al., *Expression in brain of amyloid precursor protein mutated in the*
605 *alpha-secretase site causes disturbed behavior, neuronal degeneration and premature*
606 *death in transgenic mice*. EMBO J, 1996. **15**(6): p. 1265-74.

607 41. Sensini, F., et al., *The impact of handling technique and handling frequency on laboratory*
608 *mouse welfare is sex-specific*. Scientific Reports, 2020. **10**(1).

609 42. Abe, Y., et al., *Behavioral and electrophysiological evidence for a neuroprotective role of*
610 *aquaporin-4 in the 5xFAD transgenic mice model.* *Acta Neuropathologica*
611 *Communications*, 2020. **8**(1).

612 43. Busche, M.A., et al., *Clusters of hyperactive neurons near amyloid plaques in a mouse*
613 *model of Alzheimer's disease.* *Science*, 2008. **321**(5896): p. 1686-9.

614